Tuning the selectivity on the furan-propylene Diels-Alder condensation over acid catalysts: Role of pore topology and surface acidity

Juan Gancedo, Laura Faba, Salvador Ordóñez [*]

Catalysis, Reactors & Control Research Group (CRC), Department of Chemical and Environmental Engineering, University of Oviedo, Oviedo 33006, Spain

ABSTRACT

This work is focused on obtaining aromatics from renewable resources by propylene-furan Diels-Alder condensation. Several acid catalysts with different pore topology and SiO_2/Al_2O_3 ratios were considered to gain further understanding of the molecular sieve and acidity effects on the selectivity towards different fractions and the catalytic stability. Experiments were performed in a fixed bed reactor at 500 ºC, WHSV = 17.4 h^{-1} and 3:1 propylene:furan molar ratio. Small pore-size materials (CHA, FER, MOR) are mainly selective to alkenes following cracking and oligomerization pathways, whereas materials with a larger pore size (FAU, MCM-41) produce polycyclic compounds and coke precursors. BEA and mainly MFI zeolites have the optimum topology to produce aromatics, mainly toluene. Experimental results suggest a competition between condensation and alkylation, the first one being promoted by the strongest acidic sites. These data provide the basis of a comprehensive reaction mechanism that allows anticipating the product distribution as a function of the catalytic properties of the considered material.

1. Introduction

Aromatic compounds (such as the BTX fraction: benzene, toluene, and xylenes) are essential in the current chemical industry, with global consumptions close to 100 million tons per year, with a typical BTX ratio of 4:1:3 [1,2]. They are used as essential commodities in many chemical processes, from polymer manufacturing (polyethene-terephthalate, polystyrene, polyurethanes, etc.) to fine and pharmaceutical industries. Currently, BTXs are obtained by different processes in refineries, high-lighting the catalytic reforming of naphtha and the steam cracking of hydrocarbons (pyrolysis gasoline mainly) followed by extraction steps (liquid-liquid extraction or extractive distillation) required due to the complexity of the product distribution obtained. BTX are also industri-ally produced by the oligomerization of light alkanes (mainly propane), a chemical route for the valorisation of natural gas resources and light paraffin produced in petroleum refineries [3,4].

As the processing of fossil resources is supposed to decrease in the following years, alternative routes are needed to substitute the classical ones. Looking at the low carbon footprint and the required high avail-ability of the raw material, biomass-based procedures to obtain aro-matics have deserved an increasing interest in the last years [5]. In this biorefinery context, relevant studies propose a sustainable route to

obtain light alkanes as by-products in the transesterification of bio-oil [6,7], the industrial BTX production by this path being hindered by the low alkane yields obtained. A most promising route considers the sustainable production of furans and olefins as intermediates that could be transformed into BTX by Diels-Alder reactions. These intermediates are obtained by a general biomass thermal cracking [8–10], or by another more selective chemo- and bio-catalytic pathways, such as hydrogenolysis and dehydration of glycerol (renewable route to obtain propylene) [11] or acid hydrolysis of biomass (furan compounds) [12].

Diels-Alder reaction is a cycloaddition catalysed by acidic materials in which a conjugated diene adds to dienophile, yielding a plethora of aromatic derivatives as a function of the pair of reactants used [13–15]. This route has attracted scientific attention in the last decade, with relevant contributions studying different reactants, and reaction condi-tions to optimise the selectivity towards any of the different BTX com-pounds, both in the gas and liquid phase.

In the gas phase, a maximum of 58 % of the aromatic selectivity towards toluene is reported using furan and 2 % of propylene at 600 ºC, whereas xylene is the principal aromatic obtained at 450 ºC (49 %) when substituting the furan by 2-methylfuran (MF) [15]. In a different approach, a toluene selectivity of 50 % is obtained at 550ºC co-feeding propane during the furan catalytic fast pyrolysis, in such a way that

---

propylene is in situ obtained by propane dehydrogenation, highlighting the relevant influence of the reactant ratio in the products' distribution [16]. A deep study of the temperature role in the systems furan/methylfuran and methanol (in situ production of ethylene and propylene by methylfuran cracking) indicates that p-xylene is promoted at medium temperatures (400–450 ºC, 39 %), whereas higher ones enhance the production of toluene [17] and gaseous products [18]. Specific studies involving dimethylfuran (DMF) are reported to produce p-xylene, suggesting ethylene [19], acrylic acid (productivity higher than 70 %) [20] or propylene (>15 % with an almost total isomer selectivity) [21] as possible dienophiles. p-Xylene is also the main product obtained from DMF and ethylene at 250 ºC using MFI zeolites, in this case in a liquid phase, with a maximum yield of 75.8 % after 24 h [19].

Almost all these studies consider the use of MFI as the catalyst, with only a few references regarding other materials, such as BEA zeolite [22], anticipating a key role of the pore size of the zeolite as the key parameter. This statement is the starting point of most of these works, but there is a lack of systematic screening to deeply analyse the real effect of the pore size in the activity or product distribution. In fact, despite the good activity of MFI materials, there is no agreement about the optimum conditions since the reaction produces a complex mixture of aromatics and cracking products (olefins, CO, CO_2). The pore size is also expected to have a relevant influence on this distribution, justifying the need for this screening.

On the other hand, the influence of SiO_2/Al_2O_3 ratio in the product distribution has been indicated only in the methylfuran/ethylene system [18], without other studies that allow proposing a general mechanism of this complex reaction, allowing predicting the product distribution as a consequence of the synergetic effect of the pore size and acidity of the catalyst. In addition, the reaction is strongly conditioned by a high coke production with the subsequent catalytic deactivation. In most of the studies, this deactivation is suggested to be promoted by the oligomerization of oxygenated common intermediates such as benzofuran [23, 24], but there are no references related to the coke formation route as well as the relevance of benzofuran for the furan/propylene system.

To our best knowledge, there is a gap in the literature related to the comprehensive mechanism of this reaction, with only partial studies published. Combining this study with a complete screening of different zeolites (zeotypes and acidities) is very helpful to determine the coke production routes, the required knowledge to propose reaction conditions to minimise its formation. In addition, this information is needed to tune the pore size and surface acidity of the catalysts not only for BTX synthesis but also for the production of other aromatics of industrial interest (naphthalenes, indenes, etc.).

The scope of this work is to get a comprehensive view of the furan-propylene Diels-Alder reaction, determining the roles of the catalyst pore size (studying different zeotypes: CHA, FER, MOR, MFI, BEA, FAU and MCM-41) and surface acidity (different SiO_2/Al_2O_3 ratios for BEA and MFI zeolites) on both selectivities for the different products and coke production with the subsequent effect on the catalyst deactivation, proposing a complete mechanism that allows identifying the optimum conditions to enhance the selectivity towards different target compounds: BTX; naphthalenes, indenes.

2. Materials and methods

2.1. Materials

Zeolitic materials with different topologies were tested in this study: CHA (ACS), FER, MOR, MFI, BEA and FAU (Zeolyst) and MCM-41 (Sigma Aldrich, labelled as MCM for simplicity). In addition, four different SiO_2/Al_2O_3 ratios were examined in MFI (23, 30, 50 and 80) and BEA zeolites (25, 38, 75 and 300). Their main crystallographic parameters are summarised in Table S1 of the Supplementary Information. The active forms (protonated species) were obtained by calcination in

air of the parent ammoniacal forms at 550 ºC for 12 h, the temperature reached with a 1ºC·min^{-1} slope. This thermal treatment was carried out with all the samples to ensure the same preparation procedure, including those already in their protonated form (BEA 75, BEA 300 and MCM). All the catalysts were pelletized at 3.8 tons·cm^{-2} and sieved to 250–355 μm.

2.2. Catalyst characterization

Nitrogen isotherms were determined in a Micromeritics ASAP 2020 equipment, using 100–200 mg of catalyst for each test. The t-plot method was used to determine the micropores volume and external area; BJH method for mesopores volume and pores area; and BET method to estimate the total surface area. Total pore volumes were calculated as the sum of micro and mesopores volumes. The crystallographic structure of the protonated zeolites was determined by X-ray diffraction (XRD) using a PANalytical X'pert Pro MPD with a CuKα line in the range 5 – 90º, at 0.025º·min^{-1} of scanning rate. The acidity was measured by temperature programmed desorption of ammonia, NH$_3$-TPD in an AutoChem II 2920. In a typical procedure, the catalyst surface was initially cleaned in helium flow at 300ºC for 30 min, the temperature reached with a slope of 5 ºC·min^{-1}. The acid sites saturation was done with a flow of 2.5 % NH$_3$ in helium (20 ml·min^{-1}, s.t.p) at room temperature. Once the excess of NH$_3$ was removed from the surface (2 h, 30ºC), the concentration of acidic sites was quantified by following the NH$_3$ desorption signal in a Pfeiffer Vacuum Omnistar Prisma mass spectrometer. This signal was measured whereas the catalyst was heated from 30 ºC to 950 ºC with a 5 ºC·min^{-1} rate in a flow of helium (20 ml·min^{-1}, s.t.p.). The desorption temperature allows to identify three different acid sites strengths as a function of ammonia desorption temperature [25,26].

FT-IR spectra of pyridine adsorption were carried out to measure the Lewis and Brønsted acid sites ratio (LAS/BAS) using the Eq. 1., where A_L/A_B is the ratio of the absorbance areas, and ϵ_B/ϵ_L the extinction coefficient ratio, with values of 0.73 and 1.11 cm·μmol^{-1} for ϵ_L and ϵ_B, respectively [27].

$$\frac{LAS}{BAS} = \frac{A_L}{A_B} \cdot \frac{\epsilon_B}{\epsilon_L} \tag{1}$$

IR spectra (128 scans, resolution of 2 cm^{-1}) were collected employing a Thermo Nicolet Nexus FTIR equipped with a Smart Collector Accessory and a MCT/A. Samples were pretreated at 400 ºC in He for 5 min. A background spectrum of the dry material was taken at 200ºC. Pyridine was added by dry impregnation with a controlled amount of pyridine (10 % higher than the pore volume of the material), removing the non-adsorbed pyridine by flowing He (50 ml·min^{-1}) at 200 ºC for 30 min before the spectrum [28]. The subtraction of the spectra before and after pyridine impregnation displays the pyridine absorption to the catalysts acid sites (1450 and 1540 cm^{-1} for LAS and BAS, respectively).

2.3. Catalytic studies

Samples of 15 mg of catalyst were mixed with 105 mg of glass, milled with the same particle size (250–355 μm) and placed inside a U-shaped fixed-bed quartz reactor (0.7 cm i.d.). The reactor was placed inside an electric oven with a PID temperature controller furnace equipped with a thermocouple close to the upper surface of the catalytic bed to ensure the correct temperature control. 2.5 v. % of furan (Aldrich Chemistry, >99 %) was fed using a syringe pump into a stream of 7.5 v. % of propylene (Air Liquide, >99.5 %) in helium (Air Liquide, >99.999 %), reaching a global flow of 20 Nml·min^{-1} with a total organic fraction of 10 % (WHSV=17.4 h^{-1}, propylene/furan molar ratio of 3). The reaction temperature and pressure were maintained at 500 ºC and 2.2 ± 0.1 bar, respectively. The pressure drop along the reactor was always lower than 0.1 bar. All the pipes and fittings were heated at 250 ºC with

heating blankets to avoid products' condensation and to ensure the flash vaporisation of the furan in the transfer line (furan boiling point at 2.2 bar: 56 °C). A scheme of the experimental set-up is included in the Supplementary information (Scheme S1).

A qualitative analysis was performed by gas chromatography coupled to a mass spectrometry detector (GC-MS Shimadzu QP 2010) with a TRB 5MS capillary column as stationary phase (30 m, 0.25 mm). The samples were collected by condensation of the reactor effluent in acetone and octane solvents over an ice bath. Structural isomers have been gathered into families. For simplicity, each family is represented in the reported data by the most concentrated isomer. Alkenes with six or more carbon atoms and benzenes and naphthalenes with three or more alkylation orders are also lumped into families. In addition, due to the big amount of reaction products, the results were analysed in lumped fractions: benzofuran, alkylfurans, indenes, naphthalenes, benzenes and alkenes. Each fraction includes the main compound as well as all its alkylated subproducts.

Quantitative analyses were carried out online by gas chromatography with a flame ionization detector (GC-FID HP 6890Plus) with the same capillary column as the GC-MS. Chromatograph results were analysed with calibrations using commercial samples and response factors [29]. The percentage of unknown compounds area in the chromatographs was lower than 3 % in all cases.

Initial conversions were calculated from the difference between the inlet and outlet concentration at the initial time (Eq. 2). The discrepancies in the carbon balances (CB) (Eq. 3) were assumed to be due to the formation of coke, char, condensed compounds, CO, and/or CO_2, naming this group as "Coke & CO_x". Selectivities were calculated in terms of carbon excluding the furan and propylene (Eq. 4). In the equations, "C" is the concentration and "n" is the number of carbon atoms of the reactants, "r", or every product, "i". BTX production was calculated knowing the conversion and carbon flow introduced of each reactant (F_i, mmol C·h^{-1}) and the selectivity to BTX (Eq. 5).

$$\chi = Conversion \quad (\%) = \left(1 - \frac{C_{r1}}{C_{r0}}\right) \cdot 100 \quad (2)$$

$$CB = Carbon \quad balance \quad (\%) = \frac{\sum(n_i \cdot C_i)}{\sum(n_r \cdot C_{r0} - n_r \cdot C_{r1})} \cdot 100 \quad (3)$$

$$\varphi_i = Carbon \quad selectivity \quad (\%) = \frac{n_i \cdot C_i}{\sum(n_i \cdot C_i)} \cdot CB \cdot 100 \quad (4)$$

$$\eta = BTX \quad production \quad \left(mmol\frac{C}{h}\right) = \frac{\sum(F_i \cdot \chi_i) \cdot \varphi_{BTX}}{10000} \quad (5)$$

The experimental results shown in all the manuscript correspond to the average values obtained after two replicates, observing in all the cases discrepancies lower than 3 % between equivalent experiments.

2.4. Coke characterization

Coke deposited during reactions was analysed by temperature-programmed oxidation analyses (TPO) of the spent catalysts in a Micromeritics Autochem II 2920. Initially, a He flow (20 ml·min^{-1}) was used to clean the surface. The temperature was kept at 150 °C for 30 min, using a 5 °C·min^{-1} slope to reach the set point. Coke combustion was carried out with a 5 % O_2/He flow (20 ml·min^{-1} s.t.p.), increasing the temperature from room conditions up to 950 °C, with a 2.5 °C·min^{-1} rate. The CO_2 effluent was analysed by mass spectrometry (Omnistar GSD 301).

DRIFT spectroscopy was carried out using same equipment than pyridine adsorption analyses. The fresh or spent catalyst (10 mg), depending on the experiment, was placed inside the catalytic chamber. Spectra were recorded in the 4000–650 cm^{-1} wavenumber range, after subtraction of the KBr standard background.

3. Results and discussion

3.1. Performance of the selected zeolites: conversion and selectivity trends

Different zeotypes were selected for this study, trying to cover wide ranges of porous structures. Main characterization results are summarised in Table 1, whereas the detailed results (XRD diffractograms, NH$_3$-TPD profiles and IR pyridine spectra) are included in the Supplementary Information (Fig. S1-S3).

Except for MCM, all the zeolites are microporous materials. In this context, the pore diameter is the most relevant parameter to explain the catalytic activity. A continuous distribution from 3.8 to 7.4 Å is obtained. These values correspond to XRD analyses carried out at room temperature. However, reactions will take place at 500ºC. This temperature dilates the pores significantly, in such a way that compounds larger than the crystallographic pore sizes can get in and out without being blocked inside the zeolite. The Norman radii correction, indicated in Table 1, is one of the most widespread pore size adjustments to include this effect in gas-phase catalytic reactions [30–32]. According to this hypothesis, the effective pore at this temperature is around 0.7 Å higher than the crystallographic one. Regarding the morphological parameters, the surface area of these zeolites ranges from 243 to 710 m^2·g^{-1}, with almost 970 m^2·g^{-1} in the case of the mesoporous MCM. The percentage of this area that corresponds to the external surface is lower than 10 % in the case of CHA and FER, with increasing values up to almost 40 % in the case of FAU (results summarised in Table S2). As result of both aspects, the range of internal surfaces is significantly narrower, with values from 213 to 377 m^2·g^{-1}, with the exceptions of MCM, FAU and CHA, with more than 520 m^2·g^{-1}. As to the pore volume, similar values are obtained for almost all the zeolites (0.20 – 0.26 cm^3·g^{-1}), with the exception of the largest pore material, with values up to 0.98 cm^3·g^{-1}. As expected, in zeolites, microporosity prevalence over mesoporosity, observing very similar values for all the materials, with increasing mesoporosity as the pore size of the material increases.

Similar SiO$_2$/Al$_2$O$_3$ and LAS/BAS ratios were chosen in all the cases to isolate the effect of the zeolite framework from the acidity one, except MCM. However, significant discrepancies in acidity are observed, the MFI being the catalyst with the highest concentration of these active sites (15.6 μmol NH$_3$·g^{-1}). Lower values are obtained as the pore sizes increase or decrease, this effect being more marked for FAU and MCM. Comparing all the NH$_3$-TPD profiles of all the zeolites, the strength of the acid sites was sorted considering three different intensities as a function of the ammonia desorption temperature: weak (<200 ºC), medium-strength (200–500 ºC), and strong sites (>500 ºC). In all the cases, weak sites prevail over the strong ones, this ratio being more significant for materials with pore sizes higher than 5.4 Å. Quite similar LAS/BAS

Table 1
Textural and acidic properties of the different catalysts used in this study.

	CHA	FER	MOR	MFI	BEA	FAU	MCM
SiO$_2$/ Al$_2$O$_3$ **X-Ray diffract. (XRD)**	20–30	20	20	23	25	12	79
Crystallogr. diameter (Å)	3.8	4.5	5.0	5.4	6.1	7.4	30
Norman radii correct. (Å)	4.5	5.2	5.7	6.1	6.8	8.1	30
NH$_3$-TPD (μmol NH$_3$·g^{-1})							
Weak (<200ºC)	4457	3375	5906	9598	5083	2526	440
Medium (200–500ºC)	3265	2975	4220	5416	4327	2567	510
Strong (>500ºC)	608	466	–	569	715	406	–
Total	8330	6816	10126	15583	10126	5499	950

ratios are obtained (0.23–0.5), as detailed in Table S3. According to this fact, the differences in strength are not directly related to the amount of any type of acid sites, being a direct consequence of the accessibility and location of these sites.

The initial conversions obtained during the furan and propylene reactions at 500ºC are shown in Fig. 1, demonstrating very different performances as a function of the catalysts. In general terms, furan conversion is higher than the corresponding to propylene, as anticipated considering that it is the limiting reactant. However, the ratio between both conversions is strongly dependent on the catalyst. Zeolites with the smallest pore sizes (CHA, FER, MOR) present almost the same furan and propylene conversions (33 – 35 %), values quite similar to the furan conversion ones (30 – 32 %). A complete change in trend is observed from MFI to MCM. Total furan conversion is reached with the MFI, with decreasing values (from 41 % to 29 %) at increasing pore sizes. A similar evolution is observed for the propylene, but with values significantly lower than the furan ones: from 68 % to 14 %, with MFI and MCM, respectively.

The desired condensation routes are catalysed by acid sites [9]. However, the lack of correspondence between conversions and acidity, neither total nor weak/medium/strong ones, suggests the presence of other parameters controlling the reaction performance. Results do not show any trend with respect to external morphological parameters, discarding any relevant role of mesoporosity. Differential limitations by external diffusion are discarded because of the similarity of most of the considered materials in terms of particle diameter and the presence of active sites out of the porous structure. By contrast, internal diffusion limitations, conditioned by the pore sizes, play a key role in the activity results. These statements were mathematically corroborated, obtaining external diffusion coefficients (0.0042 and 0.0049 $cm^2 \cdot s^{-1}$, for propylene and furan, respectively), six orders of magnitude higher than the internal ones. The Knudsen diffusivity is proportional to the pore size, with values from $1.5 \cdot 10^{-9}$ to $1 \cdot 10^{-8}$ $cm^2 \cdot s^{-1}$, for CHA and MCM, respectively, and the effective diffusivity coefficient directly matches with these values. Thus, the reaction is controlled by the reactants and products' mass transference in the internal porosity of these materials. The detailed procedure to calculate the diffusion coefficients is explained in the Supplementary Information, the corresponding values being summarised in Table S4.

This hypothesis justifies the conversions obtained, close to the 3/1 propylene/furan ratio for largest-pore zeolites, whereas the propylene conversion is higher than the expected one for CHA, FER and MOR zeolites. Since acid sites must catalyse both conversions, diffusional limitations in the small-pore zeolites seem to be the key aspects that control the activity.

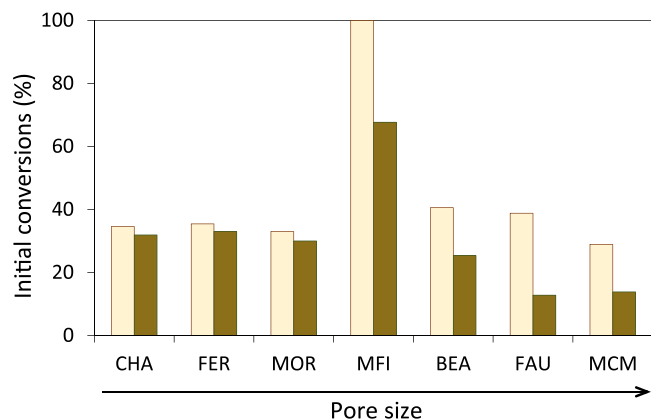A complete analysis of these results requires comparing product distribution for the different reaction products. These results are shown in Fig. 2, considering the initial selectivity to each family of compounds in carbon terms. Except in the case of MFI, all the results correspond to a narrow range of furan conversion (30–40 %). Despite the low catalytic loading used, the conversion control with MFI at this level is not easy, being affected by the deactivation (discussed below).

As in the case of conversions, the catalysts must be grouped into two different groups for discussion. Those zeolites with the smallest crystallographic pores (CHA, FER, MOR) strongly promote the formation of the alkenes (selectivities of 94 % with CHA). These alkenes derived mainly from propylene (cracking, oligomerization reactions), as it is described in Scheme 1. The prevalence of the route from alkenes has been corroborated by individual experiments feeding only propylene over MFI and BEA catalysts. The selectivity distribution, as well as the temporal evolution of conversion and carbon balance, is included in the Supplementary Information (Fig. S4). With both catalysts, alkenes are the main compounds when feeding only propylene, obtaining a size distribution proportional to the pore size. Thus, 14.8 % and 19.4 % of ethylene and butene, respectively, are obtained when using MFI, whereas the higher pore size of the BEA promotes the formation of butene over ethylene (33.5 % and 4.9 %, respectively). In the literature, the furan decarbonylation is also proposed as a route to obtain alkenes since it promotes the formation of allene, a very unstable compound that suffers fast dimerisation, obtaining propylene and large alkenes [33,34]. The hydrolysis of furan yielding CO_2 and propylene is also reported at these conditions [35]. Experimental results feeding only furan (see Fig. S4) indicate that these routes have a low influence in the total reaction, with less than 2.3 % and 0.5 %, with MFI and BEA, respectively. The relative weight of each route can change when feeding both reactants, and the quantification of their relevance is then impossible to elucidate. To sum up, all these alkenes can react by different oligomerizations and cyclizations, the extent of these reactions being limited by the pore topology.

For these small-pore size materials, alkene fraction production decreases as the pore size increases, obtaining a selectivity of 23 % with MOR. This decrease matches with a significant increase in the carbon unbalance, a label that includes the formation of CO and CO_2 as well as possible solid deposits. The analysis of this fraction and the consequences on the catalytic stability are discussed in the following section.

A clear change in trends is observed in the case of the MFI, material with which the "carbon unbalance" fraction is minimised (<10 %). High production of the most interesting compounds (benzene, toluene, and xylene) is reached, with more than 63 % of global selectivity. The second
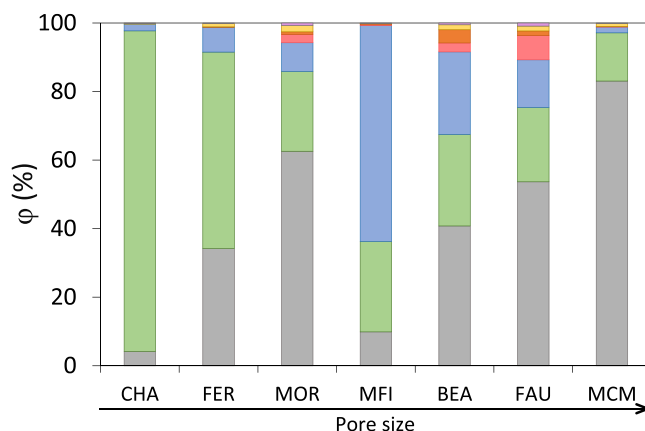

Fig. 1. . Initial conversions (TOS = 0.1 h) obtained in the furan/propylene reaction at 500 ºC using 20 ml·min^{-1}, 2.5 %v furan, 7.5 %v propylene as function of the catalyst used (15 mg). Symbols: Furan ( ) and propylene ( ).

Fig. 2. . Global carbon selectivity obtained in the furan/propylene reaction. Symbols: ( ) benzofuran, ( ) alkylfurans, ( ) naphthalenes, ( ) indenes, ( ) benzenes, ( ) alkenes, and ( ) Carbon unbalance (solid deposits and CO$_x$). *(See* Fig. 1 *for reaction conditions).*
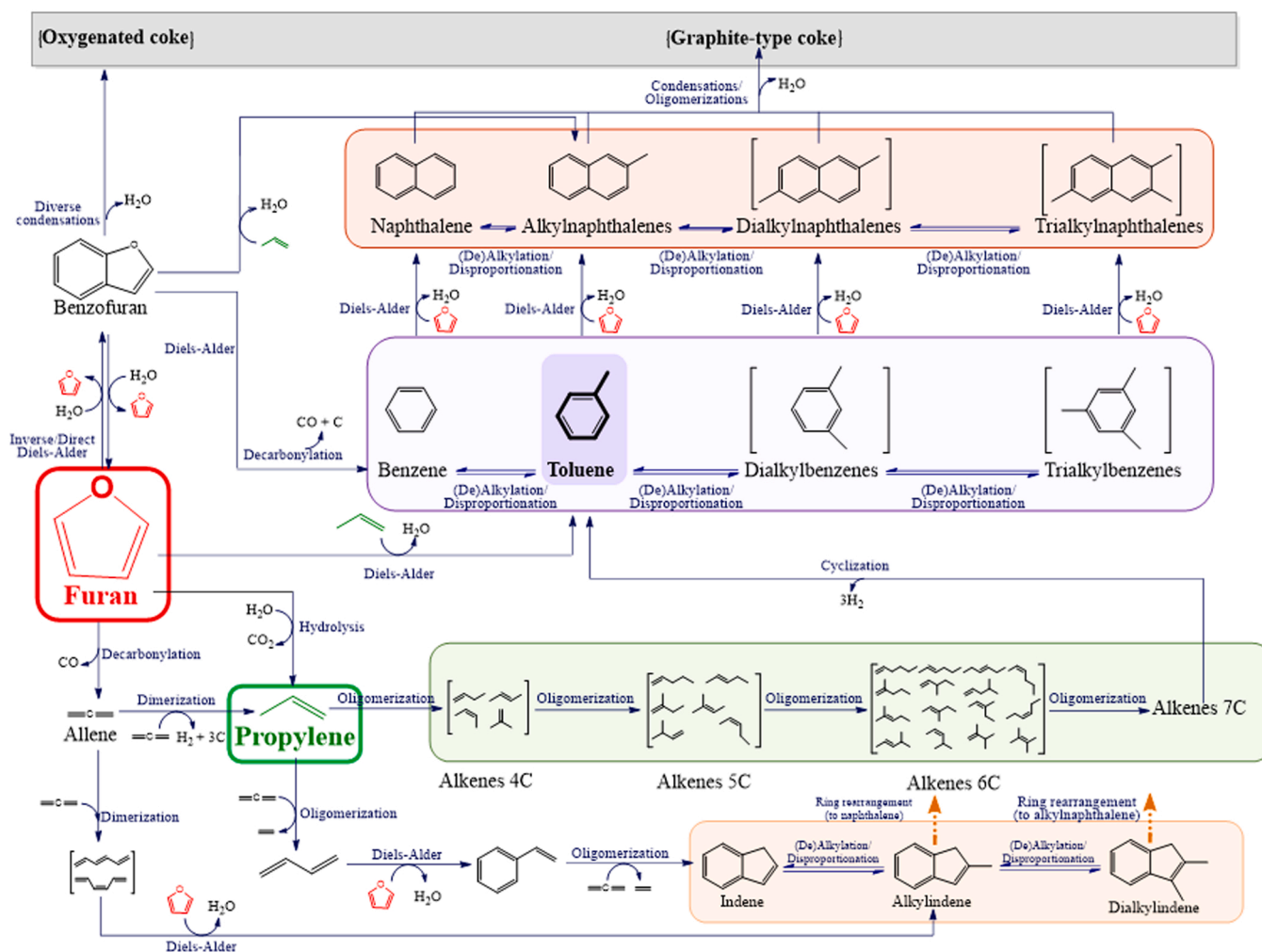
Scheme 1. . Overall mechanism proposed for the furan and propylene reaction over acid zeolites.

major fraction corresponds to alkenes, with 26 % of the carbon selectivity. Thus, the production of undesired compounds such as benzofurans, indenes and naphthalenes, identified as coke precursors because of their high size and oligomerization trend [23,36] is minimised to less than 0.7 %.

According to the mechanism proposed in Scheme 1, these results are justified in two ways: on one hand, the alkene cyclizations are more likely to take place at these conditions. However, the relevance of this route is not very high, as concluded by the negligible hydrogen concentrations detected in the gas phase. On the other hand, and proposed as the main route, the Diels-Alder reaction between furan and propylene can take place yielding toluene. This route is proposed as the main one, according to the good correspondence with both reactants' conversions. As other alkenes derived from propylene can also participate in the reaction, different branches of the aromatic structure are obtained. It should be also noted that toluene can take part in alkylation, dealkylation and disproportionation equilibria yielding benzene, xylenes, or trialkylbenzenes [37–39].

Other products observed when working with these materials are benzofuran, naphthalenes and indenes. Benzofuran is a very reactive intermediate formed by furan self-condensation, which can react yielding benzene, naphthalenes and oxygenated compounds, as determined in previous papers [24].

Naphthalenes are the heaviest coke precursors observed in the gas phase. They are mainly yielded by the Diels-Alder reaction between furan and an alkylbenzene, obtaining the corresponding alkylnaphthalene as a function of the compound involved (naphthalene from

benzene, alkylnaphthalene from toluene, etc.) [15]. In good agreement with this statement, experiments carried out feeding only furan indicate a naphthalene selectivity more than thirteen times higher than when feeding propylene (12.5 % and 0.9 %, with MFI, respectively). As in the case of monoaromatics, these compounds are in equilibrium via alkylation, dealkylation and disproportionation reactions (forming naphthalene, alkylnaphthalene and different di- and trialkylnaphthalenes).

Indenes and alkylindenes are also formed over MFI zeolites at a significant extent. The formation mechanism for these compounds remains unclear, Diels-Alder condensation between furan and hexatriene (product of two allenes condensation), and styrene oligomerization mechanisms being considered as the most likely according to the literature [23]. The relevant role of furan as the precursor of these reactions is also corroborated by the individual experiments, obtaining 4.4 % of indenes when using MFI, whereas this selectivity decreases to 0.8 % when using propylene as the reactant.

From MFI to MCM, the selectivity to BTX decreases as the pore size of the material increases, with a relevant growth of compounds involved in the "carbon unbalance" fraction. The selectivity to monoaromatics is only 24 % with the BEA, 14 % with the FAU and it is almost negligible with the mesoporous MCM. These low values are only partially explained by the production of bicyclic compounds, indenes and naphthalenes, which never reach values higher than 10 % of total selectivity. However, the formation of these compounds suggests a relevant role of carbonaceous solid compounds in the unknown fraction, due to the well-known oligomerization capacity of these aromatics. In the same way, traces of benzofuran are observed, suggesting the presence of

oxygenated carbonaceous deposits.

Considering the abovementioned interpretations about the formation of polyaromatics and other heavy compounds, it is suggested that as the pore size increases, the shape selectivity for the formation of anthracenes, phenanthrenes, pyrenes and other oxygenated analogues increases, obtaining a plethora of polycyclic aromatic hydrocarbons (PAHs). This results in the formation of a large fraction of carbonaceous deposits, as observed in the increase of carbon unbalance.

Obtained results suggest that both reactants conversion and selectivities are mainly controlled by the pore size, which is also reasonable considering that active sites are mainly located within the pores. Both processes are conditioned by a good correspondence between the pore size (once the Norman correction is applied) and the kinetic diameter of the molecules. The kinetic diameters of these molecules (σ) have been obtained from bibliography [31,40] or estimated with the Eq. 6 from their critical point temperature (T_c, in K) and critical pressure (P_c, in atm.) [41].

$$\sigma = Kinetic \quad diameter = 2.44(T_c/P_c)^{1/3} \tag{6}$$

The calculated values for any single compound detected in the gas phase are included in the Supplementary Information (Table S5). To sum up, the BTX family has kinetic diameters from 5.9 to 6.4 Å, whereas alkenes have values from 4.2 to 5.3 Å. As expected, once the number of aromatic rings increases, the kinetic diameter increases, with values from 6.0 to 7.0 Å in the case of indenes and 6.2–7.7 Å for naphthalenes. Higher diameters are only obtained for phenanthrenes, compounds directly identified as coke precursors and not identified in the gas phase. The good correspondence between these theoretical values and the selectivity distribution obtained for each zeolite is shown in Fig. 3. Although these hypotheses must be validated using computational tools, our results suggest a determining role of pore size on product distribution.

Considering the furan and propylene kinetic diameter (5.1 and 4.7 Å, respectively), these molecules can roughly go inside the internal active

sites of the catalysts with a very small pore diameter (CHA and FER). However, these materials hinder the direct reaction since the toluene has a larger diameter than these pores. Consequently, these molecules, if obtained, cannot go outside these pores. As a result, only cracking reactions can take place leading to small molecules, mainly alkenes. In good agreement with this discussion, the closest is the effective diameter of the pore to the alkenes size (4.2–5.6 Å) the most production of alkenes is obtained (Fig. 3a). Thus, the CHA zeolite (4.5 Å) has a selectivity to alkenes up to 94 %, decreasing to 57 % in the case of the FER (5.2 Å). A certain amount of alkenes is produced even with the mesoporous zeolites (14 % for MCM), suggesting that cracking and hydrolysis reactions hold up some relevance despite the zeolite's pore size.

MOR has a pore size (5.7 Å) slightly lower than the kinetic diameter of the toluene (5.9 Å), the main product obtained by the direct reaction. Reactants are exposed to the internal acidity of this zeolite, and toluene could be formed in the internal space (6.7 Å) but it cannot leave the zeolite. Thus, condensation reactions inside the pore take place, leading to the complete pore blockage. In this way, this material presents one of the highest selectivity to coke formation (up to 63 %).

The best results in terms of BTX production are achieved with MFI. Its pores (6.1 Å), slightly higher than the toluene kinetic size (5.9 Å), allow the product to leave the zeolite without promoting the abovementioned condensation reactions and the subsequent pore blockage. A non-symmetric bell curve distribution in the benzene's selectivity is obtained, in which the bell's centre is located between the values of the BTX diameters (5.9–6.4 Å) and which tail decreases softer than the bell's beginning (Fig. 3b). Similar results were obtained by Jae et al. [31], in a previous study about glucose valorisation, concluding that the best yield to aromatics is obtained with zeolites with pores in the range of 5.2–5.9 Å (effective pore size around 5.9–6.7 Å).

As the pore size increases (BEA, 6.8 Å; FAU, 8.1 Å), the selectivity to heavier products starts to be relevant, although significant benzene selectivity is still observed (24 % and 14 % respectively). Indenes formation (6.0–7.0 Å) are mainly promoted by BEA zeolite (up to 3.8 %), because of the similarity between their kinetic diameter and its pore
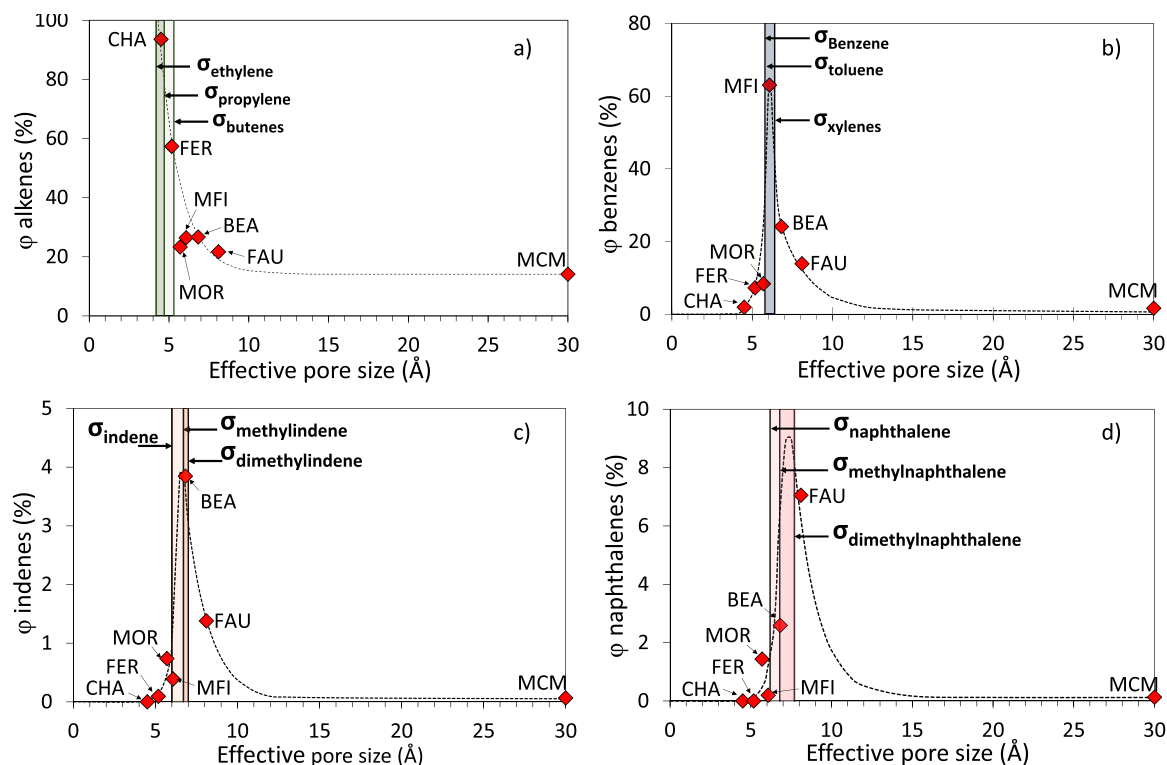

Fig. 3. . Selectivity to (a) alkenes; (b) benzenes; (c) indenes, and (d) naphthalenes analysed as function of the effective pore size of different framework zeolites. Dashed lines between experimental points serve as visual reference to indicate the estimated value of the selectivity as function of the effective pore size.

size. In this way, naphthalenes, with a slightly larger size (6.2–7.7 Å), are mainly formed on FAU zeolites (7.1 % selectivity). The selectivity distributions to these compounds correspond to a non-symmetric bell shape with the maximum in the average size of these compounds (Fig. 3c and d). Both zeolites promote the conversion of monocyclic compounds (furan and benzenes) into bicyclic compounds (naphthalenes and indenes), which are coke precursors. In good agreement with this hypothesis, these two catalysts have relevant carbon unbalances (41 % for BEA and 54 % for FAU).

On the other side, the mesoporous zeolite (MCM, 30 Å) has pores large enough that facilitate sequential Diels-Alder condensations to high boiling-point organics. These chemicals are deposited on the catalyst surface, promoting extensive coke formation. In this way, this mesoporous material produces alkenes (14 %), with a very high carbon unbalance (82 %).

The detailed distribution of the three principal reaction products families (benzenes, alkenes and naphthalenes) are plotted in Fig. 4. Although xylene (dialkylbenzene) and benzene can be obtained from

Fig. 4. . Selectivity distribution of (a) benzenes, (b) naphthalenes, and (c) alkenes obtained in the furan/propylene reaction. *(See Fig. 1 for reaction conditions)*.

toluene by disproportionation [37–39], the no equimolar xylene/-benzene ratio (xylenes/benzene ratios of 1.9, 1.6, 2.5, 1.7, 6.5, 9.9 and 3.8 for CHA, FER, MOR, MFI, BEA, FAU y MCM, respectively) suggests that this mechanism is not the predominant one. On the contrary, the formation of these alkyl derivatives is explained considering the well-known alkylation activity of propylene [42,43]. This effect is more evident in the case of BEA, FAU and MCM, the materials with the largest pore sizes, with total selectivities to these polyalkyl compounds (62 %, 61 % and 57 %, respectively), as shown in Fig. 4a. These results are congruent with previous studies published by Bellussi et al., [44], in this case studying the benzene alkylation in the liquid phase.

Looking at the naphthalenes distribution, the differences in the alkylation capacity as a function of the pore size are even more evident (Fig. 4b), without observing any of these compounds when using CHA or FER (too small pores to produce these larger molecules). With MOR, MFI, BEA and FAU, the formation of alkylated naphthalenes increases as the pore size does. In this way, MOR only produces low alkylated naphthalenes: naphthalene (59 %) and alkylnaphthalenes (41 %), whereas MFI produces a higher selectivity to alkylnaphthalenes (46 %), and a small concentration of dialkylnaphthalenes (3 %). On the contrary, alkylnaphthalenes are the main compounds when using BEA (47 %) and dialkylnaphthalenes with FAU (43 %). Trialkylnaphthalenes are only appreciable using FAU, with a selectivity of 1.8 %.

The shape selectivity also determines alkenes one (Fig. 4c). The small pore size of CHA (4.5 Å) is close to the ethylene one (4.2 Å), promoting propylene cracking over oligomerization reactions (ethylene selectivity > 67 %). Butenes and heavier alkenes (>5.3 Å) are expected to be produced mainly on the external surface of CHA: butenes (31 %) and heavier alkenes (2 %).

FER, a zeolite with a slightly larger pore diameter than the CHA (5.2 Å, same order of magnitude as the butene kinetic diameter), promotes the formation of C4 alkenes (up to 47 %), but with significant ethylene selectivity (29 %). MOR, BEA and FAU (5.7–8.1 Å) have pore sizes large enough not to present spatial constraints for heavy alkenes formation. In this way, these three catalysts have a very similar selectivity to heavy alkenes (>5 C): 36–37 %. MFI is an exception in this discussion, with a production of almost only light alkenes: ethylene (48 %) and butenes (50 %). The high selectivity to the main Diels Alder reaction, yielding toluene, seems to be the cause of this behaviour, with a predominant consumption of propylene in the main pathway. The mesoporous zeolite (MCM), with large pores (~30 Å), allows the formation of long-chain alkenes in large amounts, up to 74 %.

3.2. Catalytic stability

The formation of carbonaceous deposits is expected to be the principal deactivation cause in this reaction since many compounds have a high oligomerization capacity. These solids are considered in the initial distribution (Fig. 2) together with CO, CH_4 and CO_2 that could be obtained by different deoxygenation pathways (not quantifiable by the online analytical procedure, GC-FID). The presence of these gases was verified analysing a sample of the gas phase obtained with a gas chromatograph coupled to a thermal conductivity detector (GC-TCD). The off-line character of this analysis requires a previous sampling in which a high volume of gas is collected in a gasbag, the direct association of experimental results with the composition at a particular TOS being then not possible. According to the results obtained with MFI, the main contribution to the carbon unbalance corresponds to permanent gases (with an approximately 40 % CO_2, 25 % CO, <10 % CH_4), whereas only around 25 % would be directly related to solid deposits. The corresponding analyses with the other zeolites demonstrate a very similar gas composition, the relative weight of these gases decreasing as the catalyst pore size increases, being almost negligible in the case of MCM. In all the samples, the absence of H_2 signal suggests that alkene oligomerization and cyclization are not relevant steps to produce BTX, whereas the extent of other dehydrogenation reactions is not relevant enough for
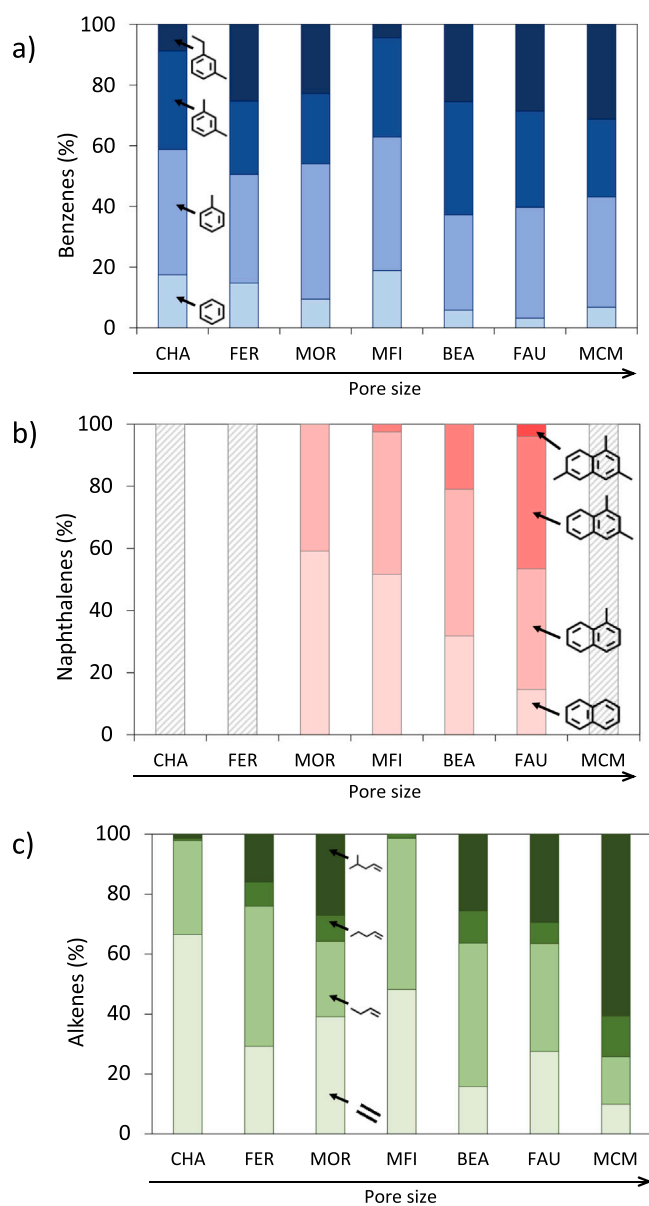
producing significant hydrogen releases.

Considering these results, the direct association of carbon unbalance with deactivation is not possible, and a correct stability discussion requires the analysis of the temporal evolution of both reactants' conversion as a function of the TOS. These results are included in the Supplementary Information (Fig. S5). A fast decrease in the propylene and furan conversions with the time-on-stream (TOS) is observed, with propylene conversions lower than 5 % in less than 90 min TOS, independently of the catalyst used. The residual conversion of furan (from 2 % to 14 %, as a function of the catalyst) could be justified by the continuous adsorption of this compound on the solid deposits or by a remaining activity once the internal porosity has been blocked.

The zone of the lineal decrease in conversion was considered to quantitatively evaluate the deactivation, taking the slope of this zone as an apparent deactivation kinetic constant. Considering that both reactants can be involved in different steps, the deactivation rates have been calculated for both compounds. Experimental values are summarised in Table 2.

As in the case of activity results, the deactivation rates must be analysed gathering the zeolites into two different groups. From CHA to MFI, both deactivation rates increase as the pore diameter does, from 0.23 and 0.29 h^{-1} with CHA, to 0.60 and 0.83 d^{-1} with MFI. The parallel evolution of both compounds suggest that deactivation is produced by compounds involving both reactants. Considering this hypothesis, as in agreement with the temporal evolution of the products distribution (Fig. S6-S12), BTX are suggested as the main deactivation promoters. Thus, from CHA to MOR, the deactivation rates increase as the BTX production does, since these zeolites present diffusional limitations for the desorption of these compounds. A particular analysis deserves MFI. The pore size of this material allows the BTX desorption, but the highest activity of this catalyst leads to a larger formation of coke intermediates (as naphthalenes or other polycyclics). In good agreement with this hypothesis, the ratio $k_{d,furan}/k_{d,ethylene}$ remains almost constant for the three smallest zeolites (1.2), increasing up to 1.4 with the MFI, which demonstrate a more relevant contribution of furan. Napthalenes, indenes, and the adsorption of furan compounds on these polyaromatic structures also trigger the deactivation of BEA and FAU, justifying the decreasing relevance of ethylene deactivation, in contrast to the increasing trend of the furan one. In any case, these values are lower than those observed for MFI. Although this lower deactivation could be positive, the very low selectivity for target compounds (mainly BTX) with these materials discards the use of these catalysts, except in the case of BEA, in which a balance between productivity and stability could be established. The anomalous results observed with MCM is justified by the different activity of this mesoporous material, demonstrating a lower activity from the first moments. The low pore density of this material reduces the deactivation rate, being deactivation caused by polyaromatics and benzofuran, since deactivation in propylene conversion is very slow. It should be noted that the analysis of these compounds is very complex due to their low volatility (if they are desorbed from the catalyst, they can condensate on the surroundings).

To gain further insights into the nature of the solid deposits, used catalysts (after 3 h TOS) were recovered and analysed by TPO and DRIFT spectroscopy. As to the TPO, the total amount of CO_2 obtained by

the combustion of the organic solids, as well as the deconvolution of the CO_2 signals is analysed in Fig. 5. The complete profiles are included in the Supplementary Information (Fig. S13). In good agreement with the previous discussion, a very low amount of CO_2 is obtained with CHA, the catalyst with which cracking is the main reaction. An increasing trend is obtained from FER to FAU, whereas a relevant decrease is observed with MCM. This unexpected result is just a consequence of its low activity (MCM shows the lowest initial conversion), leading to a low formation of coke precursors.

In general, there is a total oxidation of coke deposits at temperatures lower than 650ºC, suggesting a fluidized bed configuration for a future scale-up, taking advantage of the promising activity of fresh catalyst with a continuous regeneration to guarantee the stability. However, the comparative analysis of these materials in a fixed-bed reactor is appropriate to study the nature of these organic solids, deepening on the reaction mechanism.

As to the nature of the organic solids, two different types of deposits are observed, related to decomposition temperatures of 450–500ºC and 560–590ºC. When studying alkenes reactivity over acid zeolites, Díaz et al. [45] concluded that the first temperature interval corresponds to alkene oligomerization, a coke located outside the porous structure, whereas the second interval corresponds to coke formed within the porous structure. It should be noted that for the smallest-pore size zeolites (CHA, FER. MOR), coke formation will be mainly dependent on the alkene reactivity, this effect being not negligible for the largest-pore zeolites.

Different reactions could alter the nature of these deposits: from the participation of furan and aromatics in the reaction (more likely as pore diameter increases) to further reactions of the parent solid precursors. The first one is justified by the remaining furan conversion once no components are detected in the gas phase, suggesting a continuous accumulation of this molecule on the coke surface, leading to a bulkier coke with a lower combustion temperature, whereas the second one will lead to a denser graphitic coke with a higher combustion temperature.

Looking at the studied catalysts, a slight difference in the decomposition temperature as a function of the material is observed, with values from 580 to 590 ºC in the case of CHA, FER and MOR; and slightly lower temperatures (560–570 ºC) in the cases of MFI, BEA, FAU and MCM (Fig. S13). These results suggest that for the largest-pore zeolites (from MFI to MCM), the structure of the carbonaceous deposits is more irregular, probably by the insertion of aromatic and/or oxygenated units, leading to more reactive cokes (combustion at a lower temperature). It should be noted that these materials are also the ones with the highest selectivities to bicyclic aromatics and benzofuran, both compounds considered as coke precursors [24]. These coke structures also lead to a higher surface coverage, which increases the deactivation rate.

To gain further information about the chemical composition of these coke deposits, DRIFT experiments have been carried out. The chemical analysis by GC is not possible due to the insoluble character of the coke formed. Different organic solvents were used trying to extract the soluble coke fraction, without obtaining results in any case. Thus, the analysis without a partial thermal decomposition of its structure is not possible, whereas fluorescence effects prevent the use of Raman spectroscopy for characterizing the carbonaceous deposits. The DRIFT spectra obtained for fresh and used catalysts are shown in Fig. S14-S15, also including the signals of the fixed bed dilutant to prevent a wrong analysis of the results. As observed in Fig. S15, the lack of relevant bands in the range 3000–4000 cm^{-1} discards the presence of compounds absorbed with protic oxygen functional groups, as it could be anticipated considering the compounds involved in the reaction, as well as a relevant role of water blocking the active sites of any of the catalyst. Thus, the analysis is based on signals related to C=C and C=O absorptions. DRIFT bands associated with carbonaceous deposits are wide and complex, being congruent with the complexity of the coke formed, the identification of clear bands related to pure compounds being not possible. The almost flat spectrum of CHA is congruent with the small

Table 2
Deactivation kinetic constants obtained in the furan and propylene Diels Alder condensation at 500ºC as function of the catalyst used.

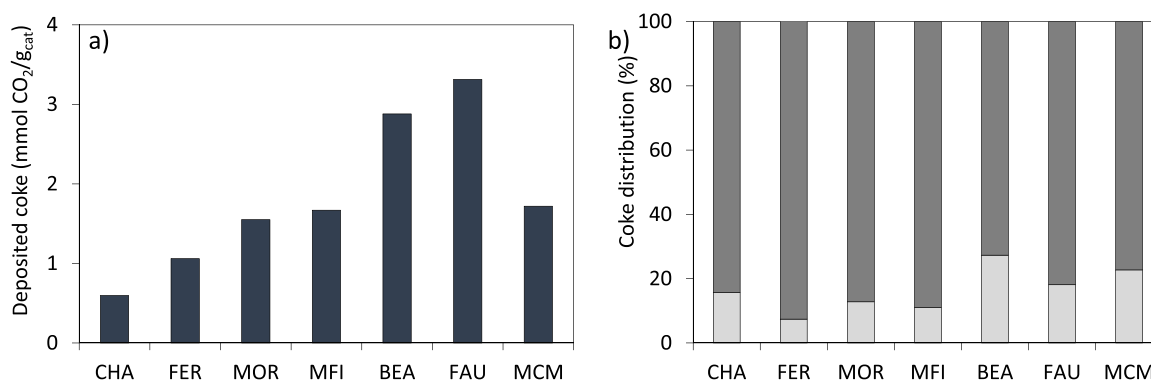|	$k_{d, propylene}$ (h^{-1})	$k_{d, furan}$ (h^{-1})
CHA	0.23	0.29
FER	0.29	0.37
MOR	0.34	0.40
MFI	0.60	0.83
BEA	0.43	0.35
FAU	0.29	0.45
MCM	0.04	0.36

Fig. 5. . TPO results analysed as function of (a) the coke amount and (b) distribution. Spent catalysts recovered after 3 h TOS of furan/propylene reaction at 500 °C. Temperatures: (■) 450–500°C, (■) 560–590 °C.

pore size of this material, and the impossibility to produce coke precursors. The spectrum of FER indicates a high proportion of graphitic coke, with signals at wavenumbers in the range 1400–1600 cm^{-1}, typical values of condensed ring aromatic structures. The spectrum of MOR, in addition to these signals, demonstrates a relevant contribution of oxygenates (aldehydes and olefin functional groups with signals in the range 1600 – 1700 cm^{-1}), suggesting a relevant role of benzofuran in the coke production. This double contribution is observed for the rest of the catalysts, with a significant decrease in the signals of spent materials. This evidence is congruent with the larger pore size of these materials, and the presence of a relevant concentration of active sites inside the channels. The deactivation of these materials is due to the blockage of this internal porosity, without observing a significant deposition on the external surface, with the corresponding decrease in the DRIFT signal and the subsequent similarity between fresh and spent materials.

As a global conclusion of the activity and stability analysis, the total production of BTX before the deactivation of MFI (1.79 g/g) is more than ten times higher than the corresponding one obtained with BEA, almost 22 times higher than with FER, MOR and FAU, and more than 50 times higher than with CHA and MCM. To sum up, the high activity of MFI is partially shielded by its low stability, whereas the BEA gathers a moderate activity with higher stability. This analysis is based on the zeolite structure, but acidity can also play a relevant role in these results. The acidity could modify the alkylation capacity of these zeolites, obtaining polyalkylated Diels-Alder products that could prevent (or decrease) the oligomerization capacity, increasing the catalytic stability. To identify the optimum acidity for this reaction, a screening of these zeolites (BEA and MFI) with different SiO$_2$/Al$_2$O$_3$ was carried out, analysing the effect in both activity and stability.

3.3. Role of the catalyst acidity on product distribution

To discuss the effect of the catalytic acidity, a detailed analysis with the two most active zeotypes using four different SiO$_2$/Al$_2$O$_3$ ratios (23,

30, 50 and 80 for MFI; 25, 38, 75 and 300 for BEA) was done. The characterization of these zeolites, shown in Table 3, reveals that there are no significant differences among the catalysts of the same type of zeolite in terms of morphology and crystallinity properties.

The XRD diffractograms and NH$_3$-TPD profiles are included in the Supplementary Information (Fig. S16-S19). As expected, the main differences are obtained in terms of acidity, with a continuous decrease in the total amount of sites as the SiO$_2$/Al$_2$O$_3$ ratio increases. This decrease occurs simultaneously with an increase in the relative strength of these sites, which also can affect the catalytic activity. IR spectra of the pyridine adsorption (Table 3, Fig. S20-S21) indicate that the LAS/BAS ratio increases as the SiO$_2$/Al$_2$O$_3$ ratio does. This way, the differences in terms of Lewis acidity are softened (2100–2900 μmol NH$_3$·g^{-1} for MFI and 2300–3800 μmol NH$_3$·g^{-1} for BEA) meanwhile the BAS show a marked exponential decrease, from 12668 to 2978 μmol NH$_3$·g^{-1} for MFI and from 6919 to 1271 μmol NH$_3$·g^{-1} for BEA (Fig. S22). It can be concluded that the influence on the total acidity of the zeolites is conditioned by the amount of BAS.

Fig. 6 shows the furan and propylene initial conversions. In the case of the MFI, no significant differences were observed, with almost total furan conversion (97–100 %) and values from 65 % to 70 % of propylene one. The maximum propylene conversion is reached with MFI (30). On the contrary, results obtained with the BEA zeolite indicate the presence of an optimum acidity. In the case of furan, the highest conversion is obtained with BEA (38), reaching 76 %, whereas the maximum of propylene conversion (44 %) is obtained with BEA (75), with a decreasing trend for both higher and lower acidities. These zeolites are those with the maximum relative amount of medium and weak acidity, respectively. These data are congruent with the presence of at least two types of reactions, one involving both reactants and another one mainly related to propylene. According to this hypothesis, the second one would require weaker acidity than the main one. The maximum propylene conversion also matches with the maximum relative amount of weak sites of the different MFI tested, but the differences are significantly

Table 3
Textural and acidic properties of the different MFI and BEA zeolites.

|	MFI				BEA			
SiO$_2$/ Al$_2$O$_3$	23	30	50	80	25	38	75	300
X-ray diffractog.								
Cryst. diameter (Å)	5.4	5.4	5.4	5.4	6.1	6.1	6.1	6.1
Norman radii correct. (Å)	6.1	6.1	6.1	6.1	6.8	6.8	6.8	6.8
NH$_3$-TPD (μmol NH$_3$·g^{-1})								
Weak (<200°C)	9598	5316	4334	2863	5083	3368	2590	1814
Medium (200–500°C)	5416	3321	2159	1415	4327	3391	1499	780
Strong (>500°C)	569	694	722	809	715	874	918	1060
Total	15583	9331	7215	5087	10126	7633	5007	3654
LAS/BAS	0.23	0.33	0.52	0.71	0.46	0.97	1.03	1.88
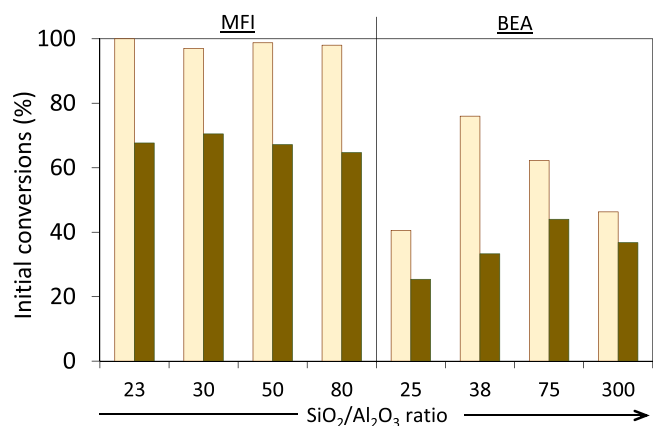
Fig. 6. . Initial conversions obtained in the furan/propylene reaction. Result corresponding to (▢) furan and (▮) propylene. *(See Fig. 1 for reaction conditions).*

lower than in the case of the BEA. This competitiveness between different reactions requires a product distribution analysis to determine the optimum material and the real role of acidity.

Fig. 7 analyses the product distribution as a function of the acidity. In the case of the MFI, a clear influence of this parameter is observed, the BTX being promoted by weak and medium-strength acidity (i.e., total acidity). The global production normalised by the acid site is almost constant (53–60 mmolC·h^{-1}·molNH$_3^{-1}$), except in the case of the most acidic one, the material with which this parameter decreases by almost 40 %. On the contrary, a slight increase in the selectivity to alkenes is obtained as the strong acidity increases (i.e., as the total acidity decreases). This strong acidity also promotes carbon unbalance. Thus, the optimum values are obtained with MFI (23). Similar trends are obtained with the BEA materials. However, the high carbon unbalances obtained with all the materials shields these evolutions, being only clearly observed when comparing the most and less acidic catalyst. With these zeolites, the lack of correspondence between BTX production and the acid sites concentration, with increasing normalised productivity and values significantly lower than those obtained with the MFIs (from 6 to 20 mmol C·h^{-1}·molNH$_3^{-1}$), indicates that tuning the activity is not enough to promote the BTX production when BEA is used as catalyst, supporting the previously discussed influence of the shape size dependence.

The acidity has a strong effect in the alkylation reactions, as observed
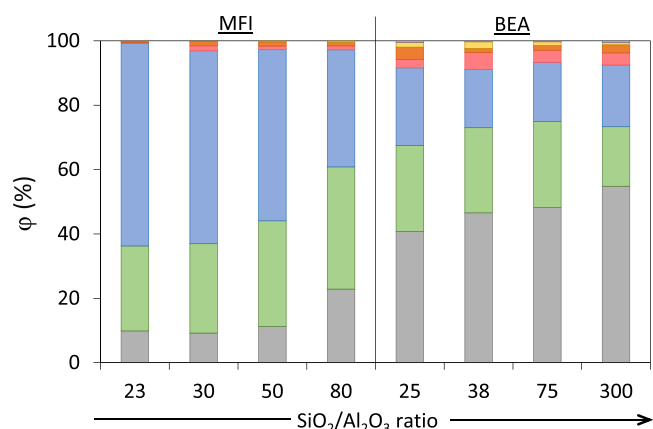

Fig. 7. . Global carbon selectivity obtained in the furan/propylene reaction as function of the acidity of MFI and BEA catalysts. Symbols: (▮) benzofuran, (▮) alkylfurans, (▮) indenes, (▮) naphthalenes, (▮) benzenes, (▮) alkenes, and (▮) Carbon unbalance (solid deposits and CO$_x$). *(See Fig. 1 for reaction conditions).*
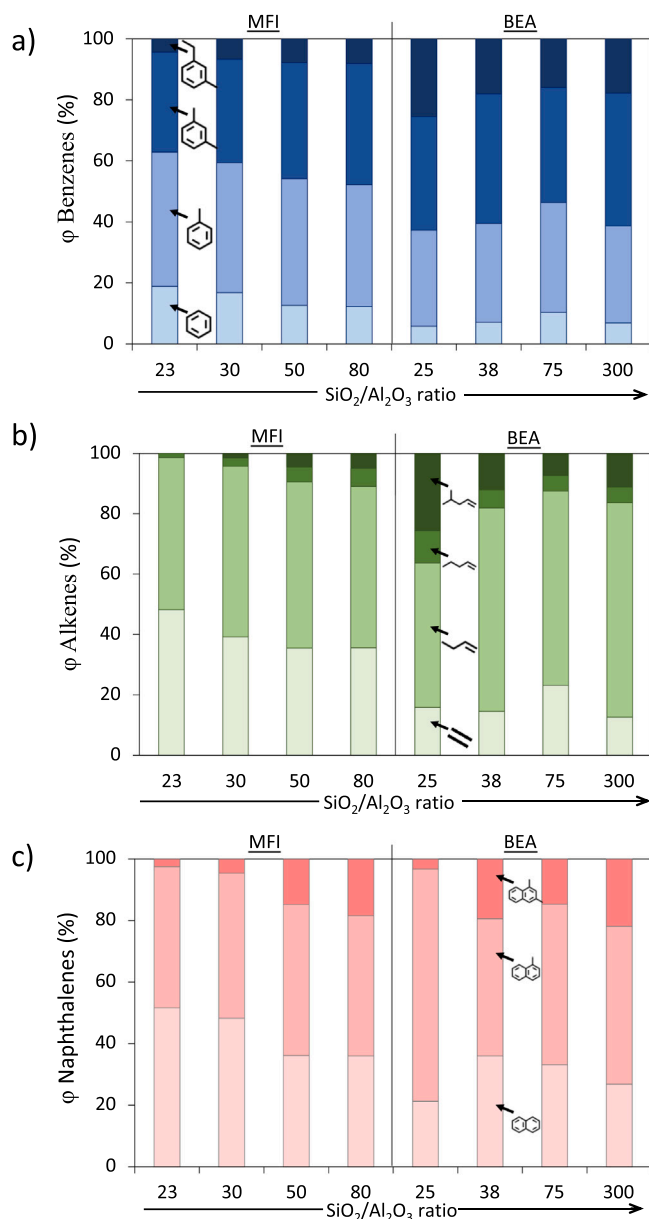

Fig. 8. . Selectivity distribution of (a) benzenes, (b) naphthalenes, and (c) alkenes obtained in the furan/propylene reaction. *(See Fig. 1 for reaction conditions).*

in Fig. 8, where the distribution of each family of compounds is detailed. In general, lower acidity promotes alkylation, this statement being clearer in the case of MFI than in the case of BEA. Thus, with MFI the relative selectivity to polyalkylbenzenes and dialkylbenzenes increases from 4 % to 8 % and 33–40 %, at the expense of alkylbenzenes and benzene (from 44 % to 40 % and 19–12 %). The same trend is observed for alkenes with more than 6 carbons (from almost 0–5 %) with the subsequent decrease in ethylene (19–12 %). The analysis of dialkylnaphthalenes is even more marked, increasing from 3 % to 18 % at the detriment of naphthalene selectivity (52–36 %). Although the same behaviour is also observed with BEA zeolites, the trends are not so clear. In any case, the results obtained with both materials suggest that alkylation is less sensitive to acidity than condensation capacity.

Acidity also plays a principal role in stability, observing a decrease in the deactivation rate as the total acidity decreases. The evolutions of conversions with TOS are detailed in the Supplementary Information (Fig. S23-S24), whereas the analysis of deactivation rates with the

acidity is analysed in Fig. 9. In the same figure, the total amount of CO_2 obtained by the TPO as well as the BTX production is also included. The TPO profiles are included in the Supplementary Information (Fig. S25) without observing disparity among the different materials tested of the same framework. It should be highlighted that the similar analysis with the different zeolites does not indicate any good correlation.

In the case of MFI, a perfect correlation between both deactivation rates and the acidity is obtained, in such a way that both values decrease as the acidity does. As anticipated, the BTX production increases with the acidity, although the improvements observed at the highest acid sites concentration is not significant. Surprisingly, the coke concentration presents a maximum at low surface acidity, with a relevant decrease for more acidic catalysts. This fact suggests that the promotion of Diels-Alder reaction with the acidity prevails over the coke formation. At first insight, these lower amounts of carbon in the most acid sample seem to be not congruent with the highest deactivation rate. It should be noted that the role of the aromatics in the formation of coke deposits will be more important in these catalysts, leading to a more disordered coke (with the presence of aromatic and olefinic moieties), which trends to occupy larger fractions of the active sites. In good agreement with this fact, the TPO profile of most acid material presents lower combustion temperatures, suggesting more disordered, reactive, and bulky carbonaceous solids (Fig. S25).

Obtained results suggest that the optimum material is MFI 30, which combines a BTX production close to the maximum (7.7 mmol·h^{-1}) with a slower deactivation than in the case of MFI (23). The same analysis with BEA is not clear since the optimum acidity to improve the BTX production corresponds to the material with the highest value of deactivation rate. In any case, the low BTX productivity, in comparison to MFI, discards the use of this material for this reaction. The lack of correspondence between these parameters and the acidity indicates that the shape selectivity prevails over the acidity, being only possible to establish correlations in terms of acidity once the optimum porosity is chosen.

4. Conclusions

Shape selectivity has demonstrated to control product distribution in the furan propylene Diels-Alder reaction over acid zeolites. CHA, FER and MOR, with a pore size lower than the BTX, present strong molecular sieve effects, promoting cracking and alkenes oligomerization reactions (ethylene and butenes as main reaction products). Zeolites with higher pore frameworks (BEA, FAU, and MCM) promote condensation these poly-cyclic compounds. Their adsorption and the continuous oligomerization by adding furan molecules justifies their fast deactivation by coke deposition.

MFI presents a slightly higher effective pore diameter (6.1 Å) than the toluene (5.9 Å), justifying its good performance in terms of conversion (100 % for furan and 68 % for propylene) and BTX formation (selectivity of 63 %). Naphthalene and indene are also produced in the internal active sites, promoting deactivation because of the product shape selectivity effect. This deactivation can be significantly reduced by promoting alkylations by controlling the acidity of these zeolites, highlighting the promising results obtained with MFI (30).

CRediT authorship contribution statement

Juan Gancedo: Investigation, Writing – original draft. **Laura Faba:** Formal analysis, Data curation, Writing – original draft, Supervision. **Salvador Ordóñez:** Conceptualization, Writing – review & editing, Supervision, Funding acquisition.

Declaration of Competing Interest

The authors declare that they have no known competing financial interests or personal relationships that could have appeared to influence
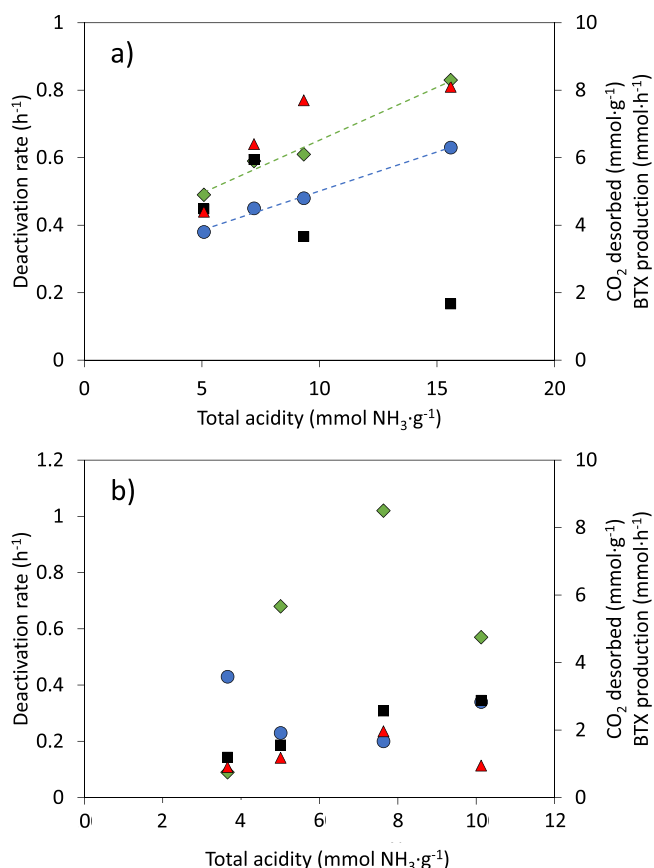

Fig. 9. Analysis of main results as function of the catalysts acidity. Results corresponding to (a) MFI and (b) BEA zeolites. Symbols: (■) furan deactivation rate; (◆) propylene deactivation rate; (●) BTX production, (▲) CO_2 determined by TPO analyses of the spent catalyst.

the work reported in this paper.

Appendix A. Supporting information

Supplementary data associated with this article can be found in the online version at doi:10.1016/j.apcata.2022.118683.

References

[1] R. Clews, Proj. Financ. Int. Pet. Ind. (2016), https://doi.org/10.1016/B978-0-12-800158-5.00011-6.
[2] M. Bender, Global aromatics supply–today and tomorrow, New Technologies and Alternative Feedstocks in Petrochemistry and Refining DGMK Conference, Drezno, 2013, 4.
[3] D.A. Wood, C. Nwaoha, B.F. Towel, J. Nat. Gas. Sci. Eng. 9 (2012) 196–208, https://doi.org/10.1016/j.jngse.2012.07.001.
[4] D. Seddon, Catal. Today 6 (1990) 351–372, https://doi.org/10.1016/0920-5861(90)85009-d.
[5] S. Wang, G. Dai, H. Yang, Z. Luo, Prog. Energ. Combust. 62 (2017) 33–86, https://doi.org/10.1016/j.pecs.2017.05.004.
[6] B. Peng, Y. Yao, C. Zhao, J.A. Lercher, Angew. Chem. 124 (2012) 2014–2017, https://doi.org/10.1002/ang.201106243.
[7] B.H. Gebreslassie, R. Wayire, F. You, AIChE J. 59 (2013) 1599–1621, https://doi.org/10.1002/aic.14075.

[8] X. Chen, Y. Chen, Z. Chen, D. Zhu, H. Yang, P. Liu, T. Li, H. Chen, J. Anal. Appl. Pyrol. 129 (2018) 53–60, https://doi.org/10.1016/j.jaap.2017.12.004.

[9] S. Kelkar, C.M. Saffron, K. Andreassi, Z. Li, A. Murkute, D.J. Miller, T.J. Pinnaviai, R.M. Kriegel, Appl. Catal. B 174–175 (2015) 85–95, https://doi.org/10.1016/j.apcatb.2015.02.020.

[10] W. Yin, R.H. Venderbosch, G. Bottari, K.K. Krawzcyk, K. Barta, H.J. Heeres, Appl. Catal. B 166–167 (2015) 56–65, https://doi.org/10.1016/j.apcatb.2014.10.065.

[11] L. Yu, J. Yuan, Q. Zhang, Y.-M. Liu, H.-Y. He, K.-N. Fan, Y. Cao, ChemSusChem 7 (3) (2013) 743–747, https://doi.org/10.1002/cssc.201301041.

[12] P. Rapado, L. Faba, S. Ordóñez, Bioresour. Technol. 321 (2021), 124500, https://doi.org/10.1016/j.biortech.2020.124500.

[13] A.E. Settle, L. Berstis, N.A. Rorrer, Y. Roman-Leshkóv, G.T. Beckham, R. M. Richards, D.R. Vardon, Green. Chem. 19 (2017) 3468–3492, https://doi.org/10.1039/C7GC00992E.

[14] J. Gancedo, L. Faba, S. Ordóñez, ACS Sustain. Chem. Eng. 10 (2022) 3057–3065, https://doi.org/10.1021/acssuschemeng.1c08544.

[15] Y.-T. Cheng, G.W. Huber, Green. Chem. 14 (2012) 3114–3125, https://doi.org/10.1039/C2GC35767D.

[16] X. Qi, W. Fan, ACS Catal. 9 (2019) 2626–2632, https://doi.org/10.1021/acscatal.8b04859.

[17] L. Zhu, M. Fan, Y. Wang, S. Wang, Y. He, Q. Li, J. Chem. Technol. Biotechnol. 94 (2019) 2876–2887, https://doi.org/10.1002/jctb.6090.

[18] C. Wang, Z. Si, X. Wu, W. Lv, K. Bi, X. Zhang, L. Chen, Y. Xu, Q. Zhang, L. Ma, J. Anal. Appl. Pyrol. 139 (2019) 87–95, https://doi.org/10.1016/j.jaap.2019.01.013.

[19] J.-C. Kim, T.-W. Kim, Y. Kim, R. Ryoo, S.-Y. Jeong, C.-U. Kim, Appl. Catal. B 206 (2017) 490–500, https://doi.org/10.1016/j.apcatb.2017.01.031.

[20] J.A.M. Mesa, F. Brandi, I. Shekova, M. Antonietti, M. Al-Naji, Green. Chem. 22 (2020) 7398–7405, https://doi.org/10.1039/D0GC01517B.

[21] Y.T. Cheng, Z. Wang, C.J. Gilbert, W. Fan, G.W. Huber, Angew. Chem. 124 (2012) 11259–11262, https://doi.org/10.1002/ange.201205230.

[22] S.K. Green, R.E. Patet, N. Nikbin, C.L. Williams, C.C. Chang, J. Yu, R.J. Gorte, S. Caratzoulas, W. Fan, D.G. Vlachos, P.J. Dauenhauer, Appl. Catal. B 180 (2016) 487–496, https://doi.org/10.1016/j.apcatb.2015.06.044.

[23] Y.-T. Cheng, G.W. Huber, ACS Catal. 1 (2011) 611–628, https://doi.org/10.1021/cs200103j.

[24] J. Gancedo, L. Faba, S. Ordóñez, Appl. Catal. A 611 (2021), 117980, https://doi.org/10.1016/j.apcata.2020.117980.

[25] J. Luo, F. Gao, K. Kamasamudram, N. Currier, C.H.F. Peden, A. Yezerets, J. Catal. 348 (2017) 291–299, https://doi.org/10.1016/j.jcat.2017.02.025.

[26] S.W. Choi, W.G. Kim, J.S. So, J.S. Moore, Y. Liu, R.S. Dixit, J.G. Pendergast, C. Sievers, D.S. Sholl, S. Nair, C.W. Jones, J. Catal. 345 (2017) 113–123, https://doi.org/10.1016/j.jcatal.2016.11.017.

[27] J. Datka, A.M. Turek, J.M. Jehng, I.E. Wachs, J. Catal. 135 (1992) 186–199, https://doi.org/10.1016/0021-9517(92)90279-Q.

[28] Z. Tai, M.A. Isaacs, L.J. Durndell, C.M.A. Parlett, A.F. Lee, K. Wilson, Mol. Catal. 449 (2018) 137–141, https://doi.org/10.1016/j.mcat.2018.02.021.

[29] J.T. Scanlon, D.E. Willis, J. Chromatogr. Sci. 23 (1985) 333–340, https://doi.org/10.1093/chromsci/23.8.333.

[30] M. Cook, W. Conner, How big are the pores of zeolites, Proceedings of the 12th International Zeolite Conference, Materials Research Society Baltimore, MD, 1999, pp. 409.

[31] Y. Wang, X. Yang, H. Zheng, X. Li, Y. Zhu, Y. Li, Mol. Catal. 463 (2019) 130–139, https://doi.org/10.1016/j.mcat.2018.11.022.

[32] J. Jae, G.A. Tompsett, A.J. Foster, K.D. Hammond, S.M. Auerbach, R.F. Lobo, G. W. Huber, J. Catal. 279 (2011) 257–268, https://doi.org/10.1016/j.jcat.2011.01.019.

[33] M. Zhou, L. Cheng, B. Liu, L.A. Curtiss, R.S. Assary, Ind. Eng. Chem. Res. 58 (2019) 15127–15133, https://doi.org/10.1021/acs.iecr.9b01969.

[34] Y.T. Cheng, J. Jae, J. Shi, W. Fan, G.W. Huber, Angew. Chem. Int. Ed. 51 (2012) 1387–1390, https://doi.org/10.1002/anie.201107390.

[35] C.J. Gilbert, J.S. Espindola, W.C. Conner Jr., J.O. Trierweiler, G.W. Huber, ChemCatChem 6 (2014) 2497–2500, https://doi.org/10.1002/cctc.201402390.

[36] E.A. Uslamin, N. Kosinov, G.A. Filonenko, B. Mezari, E. Pidko, E.J. Hensen, ACS Catal. 9 (2019) 8547–8554, https://doi.org/10.1021/acscatal.9b02259.

[37] T. Odedairo, R. Balasamy, S. Al-Khattaf, J. Mol. Catal. A 345 (2011) 21–36, https://doi.org/10.1016/j.molcata.2011.05.015.

[38] B. Mitra, D. Kunzru, Chem. Eng. Process. 64 (2013) 48–56, https://doi.org/10.1016/j.cep.2012.10.016.

[39] M. Albahar, C. Li, V.L. Zholobenko, A.A. Garforth, Micro Mesoporous Mat. (2020), 110221, https://doi.org/10.1016/j.micromeso.2020.110221.

[40] S.M. Auerbach, K.A. Carrado, P.K. Dutta, Handbook of Zeolite Science and Technology, CRC Press, 2003.

[41] R.B. Bird, W.E. Stewart, E.N. Lightfoot, N. Y. 413 (1960).

[42] T.F. Degnan Jr., C.M. Smith, C.R. Venkat, Appl. Catal. A 221 (2001) 283–294, https://doi.org/10.1016/S0926-860X(01)00807-9.

[43] J. Aguilar, A. Corma, F. Melo, E. Sastre, Catal. Today 55 (2000) 225–232, https://doi.org/10.1016/S0920-5861(99)00250-3.

[44] G. Bellussi, G. Pazzuconi, C. Perego, G. Girotti, G. Terzoni, J. Catal. 157 (1995) 227–234, https://doi.org/10.1006/jcat.1995.1283.

[45] M. Díaz, E. Epelde, J. Valecillos, S. Izaddoust, A.T. Aguayo, J. Bilbao, Appl. Catal. B 291 (2021), 120076, https://doi.org/10.1016/j.apcatb.2021.120076.